Inverse Scattering of Dielectric Cylindrical Target Using Dynamic Differential Evolution and Self-Adaptive Dynamic Differential Evolution

Chi-Hsien Sun,[1] Chien-Ching Chiu[2]

[1] Department of Electronic Engineering, National Taiwan University of Science and Technology, Taipei, Taiwan, Republic of China
[2] Electrical Engineering Department, Tamkang University, Tamsui, Taiwan, Republic of China

Received 29 May 2012; accepted 31 August 2012

ABSTRACT: The inverse problem under consideration is to reconstruct the characteristic of scatterer from the scattering *E* field. Dynamic differential evolution (DDE) and self-adaptive dynamic differential evolution (SADDE) are stochastic-type optimization approach that aims to minimize a cost function between measurements and computer-simulated data. These algorithms are capable of retrieving the location, shape, and permittivity of the dielectric cylinder in a slab medium made of lossless materials. The finite-difference time-domain (FDTD) is employed for the analysis of the forward scattering. The comparison is carried out under the same conditions of initial population of candidate solutions and number of iterations. Numerical results indicate that SADDE outperforms the DDE a little in terms of reconstruction accuracy. Int J RF and Microwave CAE 23:579–585, 2013.

Keywords: inverse scattering; computational electromagnetics; time domain; finite difference time domain (FDTD); subgridding; dynamic differential evolution (DDE); self-adaptive dynamic differential evolution (SADDE)

I. INTRODUCTION

The inverse scattering scattering problem of unknown objects has many applications including microwave imaging, nondestructive evaluation, and biomedical engineering. Numerous inverse problem techniques for 2-dimensional or 3-dimensional targets were reported [1–11]. For example, single frequency plane waves at a fixed angle were used in [1] to illuminate the perfect electric conductors (PEC), and the observation domain was located in the far zone.

Several 2D works were published, for example, the inverse scattering of 2D targets was addressed in [6, 7] using a Newton-Kantorovitch method. The application of the unrelated illumination method for 2D microwave imaging was investigated in [8, 9]. Multiscaling was applied for microwave imaging as reported in [10, 11]. However, these papers are focused on frequency-domain. As compared with frequency-domain approach, the interaction of the entire medium in the time domain with the incident field needs to be considered. In contrast, time-domain approaches can exploit causality to limit the region of inversion, potentially reducing the number of unknowns. Time-domain microwave imaging can enhance the reconstruction resolution of nondispersive scatterers and it is also capable to reconstruct the spatial distribution of the characteristic parameters of the scatterers.

The genetic algorithm (GA) was reported for shape reconstruction problems [12]. However, large amount of computation load was generally needed. Improvements in the GA were reported in [13] where good reconstruction results were demonstrated using fewer searching time. Optimization methods, such as the synchronous particle swarm optimization (SPSO) techniques were reported in [14] where the shape of 2D PEC target was reconstructed using the asynchronous particle swarm optimization (APSO). In the 2010, the dynamic differential evolution (DDE) was first proposed to deal with the shape reconstruction of homogeneous dielectric cylinders under time domain [15]. The DDE algorithm is a potentially trend to

Correspondence to: C.-C. Chiu; e-mail: chiu@ee.tku.edu.tw.
DOI 10.1002/mmce.20692
Published online 22 November 2012 in Wiley Online Library (wileyonlinelibrary.com).

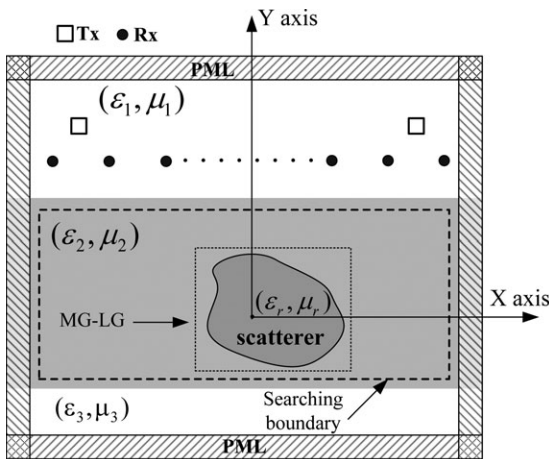

Figure 1 Geometry for the inverse scattering of a dielectric cylinder of arbitrary shape in slab medium.

obtain the global optimum of a functional whatever the initial guesses are. In recent decade years, some papers have compared different algorithm in inverse scattering [16–21].

However, these methods present certain drawbacks usually related to the intensive computational effort they demand to achieve the global optimum and the possibility of premature convergence to a local optimum. Hence, it is seemingly natural to use evolutionary algorithms, not only for finding solutions to a problem but also for tuning these algorithms to the particular problem. The proof of convergence of evolutionary algorithms (EAs) with self-adaptation is difficult because control parameters are changed randomly and the selection does not affect their evolution directly [22]. Self-adaptive differential evolution (SADE) to real-valued antenna and microwave design problems was investigated [23]. To the best of our knowledge, there are still no numerical results by SADDE to reconstruct the dielectric cylindrical target in the slab medium. Moreover, a comparative study about the performances of SADDE and DDE to inverse scattering problems is also investigated.

This work focuses on comparing these two methods for inverse scattering problems under time domain. The forward problem is solved by the FDTD method, for which the subgridding technique [24] is implemented to closely describe the fine structure of the cylinder. The inverse problem is formulated into an optimization one, and then the global searching DDE and SADDE are used to search the parameter space. Cubic spline interpolation technique [25] is employed. In section II, the subgridding FDTD method for the forward scattering are presented. In sections III and IV, inverse problem and the numerical results of the proposed inverse problem are given, respectively. Finally, in section V some conclusions are drawn for the proposed time domain inverse scattering.

II. FORWARD PROBLEM

Consider a 2D homogeneous dielectric cylinder buried in a slab medium material medium as shown in Figure 1. The cylinder is parallel to z axis buried below a planar interface separating three homogeneous spaces: the air (ε_1, μ_1), the earth (ε_2, μ_2) and air (ε_3, μ_3). The cross section of the object is star-like shape that can be representation in polar coordinates in the x-y plane with respect to the center position $(\mathrm{X_O}, \mathrm{Y_O})$. The permittivity and permeability of the buried dielectric object are denoted by $(\varepsilon_\mathrm{r}, \mu_\mathrm{r})$, respectively. The computational domain is discretized by using Yee cells [26]. It should be mentioned that the computational domain is surrounded by optimized absorber of the perfect matching layer (PML) [27] to reduce the reflection from the environment PML interface.

The direct scattering problem is to calculate the scattered electric fields while the shape, location and permittivity of the scatterer is given. The shape function $F(\theta)$ of the scatterer is described by the trigonometric series in the direct scattering problem

$$F(\theta) = \sum_{n=0}^{N/2} B_n \cos(n\theta) + \sum_{n=1}^{N/2} C_n \sin(n\theta) \qquad (1)$$

To closely describe the shape of the cylinder for both the forward and inverse scattering procedure, the subgridding technique is implemented in the FDTD code. More detail on the FDTD-Subgridding scheme and how to apply into inverse scattering can be found in [13–15].

III. INVERSE PROBLEM

A. Inverse Problem

For the inverse scattering problem, the shape, location, and permittivity of the dielectric cylinder are reconstructed by the given scattered electric field obtained at the receivers. This problem is resolved by an optimization approach, for which the global searching scheme DDE and SADDE are employed to minimize the following cost function (CF):

$$CF = \frac{\sum_{n=1}^{N_i} \sum_{m=1}^{M} \sum_{q=0}^{Q} \left| E_z^{\exp}(n, m, q\,\Delta t) - E_z^{\mathrm{cal}}(n, m, q\,\Delta t) \right|}{\sum_{n=1}^{N_i} \sum_{m=1}^{M} \sum_{q=0}^{Q} \left| E_z^{\exp}(n, m, q\,\Delta t) \right|} \qquad (2)$$

Where $E_z^{\exp}$ and E_z^{cal} are experimental electric fields and the calculated electric fields, respectively. The N_i and M are the total number of the transmitters and receivers, respectively. Q is the total time step number of the recorded electric fields.

DDE and self-adaptive dynamic differential evolution (SADDE) start with an initial population of potential solutions that are composed by a group of randomly generated individuals which represent the center position and the geometrical radii of the cylinder. Each individual is a H-dimensional vector consisting of H optimization parameters. The initial population may be expressed by $\{\mathrm{X}_j : j = 1, 2, \cdots, Np\}$, where Np is the population size. The explicit expression for X_j is given in next section. The details of the DDE and SADDE are given below.

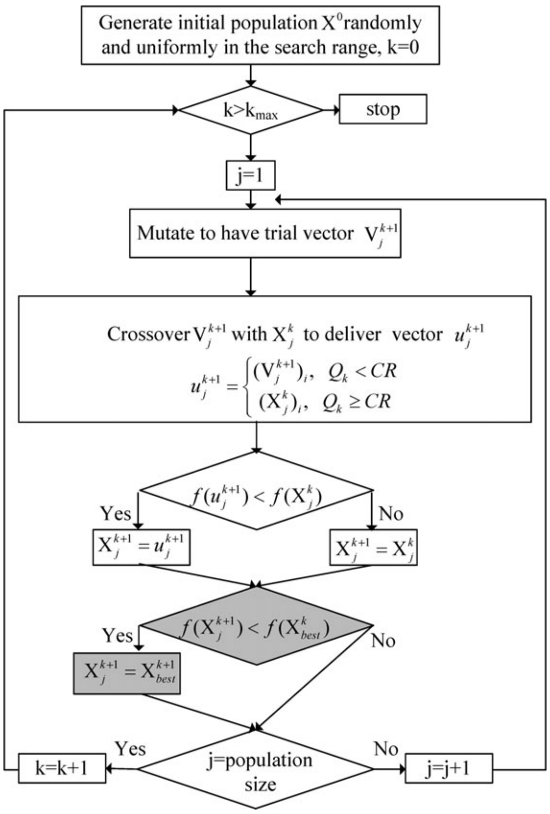

Figure 2 The flowchart of the dynamic differential evolution (DDE).

B. Dynamic Differential Evolution

In DDE, after generating the initial population, the candidate solutions are refined by applying mutation, crossover and selection, iteratively. The flowchart of the DDE algorithm is shown in Figure 2. In this strategy, a mutant vector for each target vector V_j^{k+1} at the $k+1$ generation is computed by

$$(V_j^{k+1})i = (X_j^k)i + \zeta \cdot [(X_{\text{best}}^k)i - (X_j^k)i] + \chi \cdot [(X_m^k)i - (X_n^k)i], \quad j, m, n \in [0, N_p - 1],\ m \neq n \tag{3}$$

where $i = 1 \sim D$ and χ and ζ are the scaling factors associated with the vector differences $(X_{\text{best}}^k - X_j^k)$ and $(X_m^k - X_n^k)$, respectively. The disturbance vector V due to the mutation mechanism consists of parameter vector X_j^k, the best particle X_{best}^k and two randomly selected vectors. As comparison, the mutant vector V_j^{k+1} is generated according to Eq. (4) for typical DE [28].

$$(V_j^{k+1})i = (X_j^k)i + \chi \cdot [(X_m^k)i - (X_n^k)i] \quad j, m, n \in [0, N_p - 1],\ m \neq n \tag{4}$$

where $i = 1 \sim H$ and χ is the scaling factor associated with the vector difference $(X_m^k - X_n^k)$. Note that ζ is set to zero for DE, therefore, the main differences between DDE and DE is that DDE includes the idea of approaching the ''Best'' during the course of optimization procedure.

After mutation, the crossover operator is applied to generate another kind of new vector u_j. The crossover operation in DDE delivers the crossover vector u_j^{k+1} by mixing the components of the current vector X_i and the above mutant vector V_i. It can be expressed as:

$$u_j^{k+1} = \begin{cases} (V_j^{k+1})_i, & Q_k < CR \\ (X_j^k)_i, & Q_k \geq CR \end{cases} \tag{5}$$

where $i = 1 \sim H$ and Q_k is a random number uniformly distributed within $[0, 1]$. $CR \in (0, 1)$ is a predefined crossover rate. DDE uses a greedy selection operator that is defined by

$$X_j^{k+1} = \begin{cases} u_j^{k+1}, & \text{if } CF(u_j^k) < CF(X_j^k) \\ X_j^k, & \text{otherwise} \end{cases} \tag{6}$$

Selection operation is conducted by comparing the parent vector X_j^{k+1} with the crossover vector u_j^{k+1}. The vector with smaller objective function (OF) value is selected as a member for the next generation.

C. Self-Adaptive Dynamic Differential Evolution

Storn has suggested [28] to choose the differential evolution control parameters χ and CR from the intervals $[0.5, 1]$ and $[0.8, 1]$, respectively and to set $Np = 10H$. But the suitable parameter value is, frequently, problem-dependent. The control parameters that work fine for one problem may fail to lead to convergence for other problems. The effort of trial-and-error to fine tune the control parameter is unavoidable usually. In some cases, the effort and time for this trial-and-error is unacceptable. In [22, 23] novel strategy is proposed for the self-adapting of control parameters for DE. The basic idea is to have the control parameters evolve through generations. New vectors are generated by using the evolved values of the control parameters. These new vectors are more likely to survive and produce offspring during the selection procedure. In turn, the survived vectors carry the improved values of the control parameters to the next generation. Therefore, the control parameters are self-adjusted in every generation for each individual according to the following scheme:

$$\zeta_{i,k+1} = \begin{cases} \zeta_l + rand_1 * \zeta_u, & \text{if } rand_2 < 0.1 \\ \zeta_{i,k}, & \text{otherwise} \end{cases} \tag{7}$$

$$\chi_{i,k+1} = \begin{cases} \chi_l + rand_3 * \chi_u, & \text{if } rand_4 < 0.1 \\ \chi_{i,k}, & \text{otherwise} \end{cases} \tag{8}$$

$$CR_{i,k+1} = \begin{cases} rand_5, & \text{if } rand_6 < 0.1 \\ CR_{i,k}, & \text{otherwise} \end{cases} \tag{9}$$

where $rand_1$, $rand_2$, $rand_3$, $rand_4$, $rand_5$ and $rand_6$ are random numbers with the values uniformly distributed between 0 and 1. ζ_l, ζ_u, χ_l, and χ_u are the lower and the upper limits of ζ and χ, respectively .Both ζ_l and χ_l are set to 0.1 and both ζ_u and $\chi_u$are set to 0.9 [22, 23]. The performance of SADE applied to several low-dimensional benchmark functions is reported. It is concluded that the self-adaptive strategy is better (or at least comparable) to the classical DE strategy regarding the quality of the solutions obtained. The algorithm of SADDE is a self-adaptive version of DDE, which is processed of self-adaptibility and the ability of approaching the "Best". On the basis of the self-adaptive concept, the parameters ζ, χ, and CR adjust automatically while the time complexity does not increase.

D. Cubic Spline Representation for the Cross Section of Scatterers

There are two main advantages for cubic-spline expansion as following: (i) For complicated shape, the number of unknowns for expanding the shape function by cubic-spline expansion is less than that by Fourier series expansion. (ii) The exact center of the object is insensitive for cubic-spline expansion unlike for Fourier series expansion. If there is some displacement for the exact center of the object, the number of unknowns for expanding the shape function by Fourier series expansion will increase largely. On the other hand, the number of unknowns does not vary for cubic-spline expansion [29, 30].

As shown in Figure 3, the cubic spline consists of connected curve segments described by the polynomials of degree 3 $P_i(\theta)$, $i = 1, 2, \cdots, N$. The connected segments satisfy the following continuous conditions:

$$\begin{gathered} P_i(\theta_i) = P_{i+1}(\theta_i) \equiv \rho_i \\ P'_i(\theta_i) = P'_{i+1}(\theta_i) \quad i = 1, 2, \cdots, N \\ P''_i(\theta_i) = P''_{i+1}(\theta_i) \end{gathered} \tag{10}$$

and

$$\begin{gathered} P_1(\theta_0) = P_N(\theta_N) \\ P'_1(\theta_0) = P'_N(\theta_N) \equiv \rho'_N \\ P''_1(\theta_0) = P''_N(\theta_N) \end{gathered} \tag{11}$$

Through the interpolation of the cubic spline, an arbitrary smooth cylinder can be easily described through the radius parameters $\rho_1, \rho_2, \ldots, \rho_N$ and the slope ρ'_N. As long as $\rho_1, \rho_2, \ldots, \rho_N$ and ρ'_N are given, the continuous conditions can yield a system of algebraic equations to determine all the polynomials of degree 3. By combining the optimization algorithms and the cubic spline interpolation technique, we are able to reconstruct the microwave image efficiently.

IV. NUMERICAL RESULTS

As shown in Figure 1, the 405 mm $\times$ 405 mm rectangular problem space is divided in 68×68 grids with the grid size $\Delta x = \Delta y = 5.95$ mm. The dielectric cylinder is buried in lossless slab medium ($\sigma_1 = \sigma_2 = \sigma_3 = 0$). The transmitters and receivers are placed in free space above the homogeneous dielectric. The permittivities in region 1, region 2 and region 3 are characterized by $\varepsilon_1 = \varepsilon_0$, $\varepsilon_2 = 10\varepsilon_0$ and $\varepsilon_3 = \varepsilon_0$, respectively, while the permeability μ_0 is used for each region, i.e., only nonmagnetic media are concerned here.

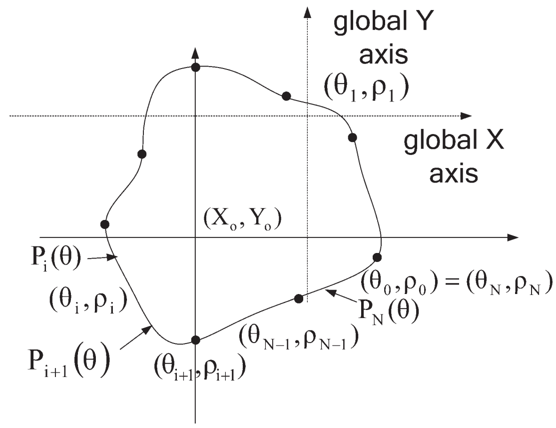

Figure 3 A cylinder of arbitrary shape is described in terms of a closed cubic spline.

The scatterer is illuminated by plane waves with the electric field polarized along the axis, while the time dependence of the field is of a one derivative Gaussian pulse. The cylindrical object is illuminated by a transmitter at two different positions, $N_i = 2$, which are located at the (-143 mm, 178.5 mm) and (143 mm, 178.5 mm), respectively. The scattered E fields for each illumination are collected at the eight receivers, $M = 8$, which are equally separated by 47.8 mm along the distance of 48 mm from the interface between regions 1 and 2. For the forward scattering, the E fields generated by the FDTD with finer subgrids are used to mimic the experimental data in (2). The proposed inversion procedures are implemented through some home-made Fortran programs that runs on an Intel PC (3.4 GHz/ 2G memory/500 G). The typical CPU time needed for DDE and SADDE examples are about 11 h in this study.

Two examples are investigated for the inverse scattering of the proposed structure by using the DDE and SADDE. There are 12 unknown parameters to retrieve, which include the center position (X_O, Y_O), the radius ρ_i, $i = 1, 2, \ldots, 8$ of the shape function and the slope ρ'_N plus the relative permittivity of the object. The parameters and the corresponding searching ranges are listed follows: $-208.3mm \le X_O \le 208.3mm, -137.8mm \le Y_O \le 137.8mm, 5.95mm \le \rho_i \le 71.4mm$, $i = 1, 2, \ldots, 8$, $-2 \le \rho'_N \le 2$ and $1 \le \varepsilon_r \le 16$. The relative coefficient of the modified DDE and SADDE are set as below: The crossover rate is 0.8. Both parameters ξ and χ are set to be 0.8. The population size is set to be 110. Here relative error for shape function and permittivity are defined as

$$\text{RelativeErrorforshapefunction} = \{\frac{1}{N'} \sum_{i=1}^{N'} [F^{\text{cal}}(\theta_i) - F(\theta_i)]^2 / F^2(\theta_i)\}^{1/2} \times 100\% \tag{12}$$

$$\text{RelativeErrorforPermittivity} = \frac{\left|\varepsilon_r^{\text{cal}} - \varepsilon_r\right|}{\varepsilon_r} \tag{13}$$

where the N' is set to 720.

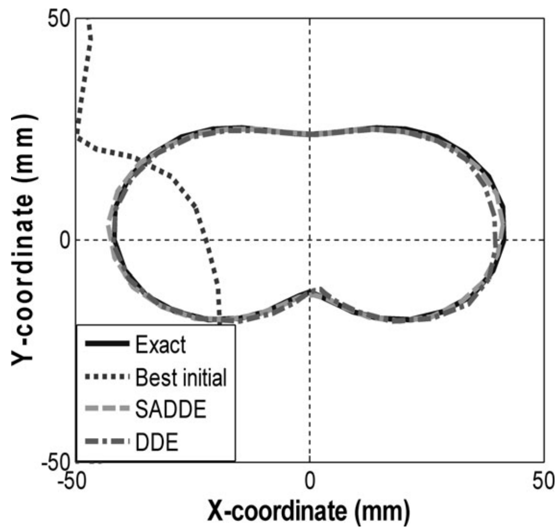

Figure 4 The reconstructed shapes of the cylinder for example 1.

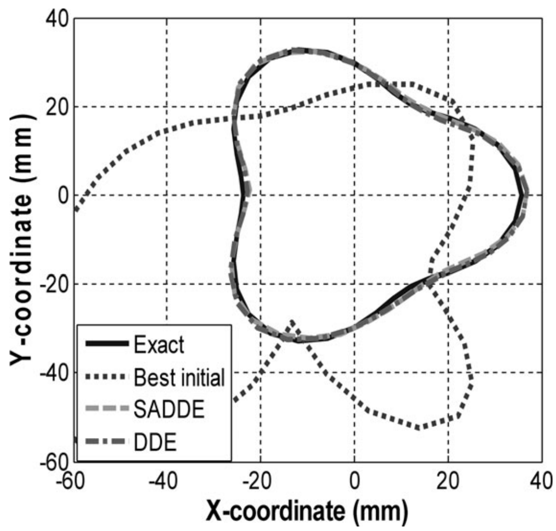

Figure 6 The reconstructed shapes of the cylinder for example 2.

In the first example, we would like to test the robustness of the algorithm. The dielectric cylinder with shape function $F(\theta) = 29.75 + 11.9\cos(2\theta) + 5.95\sin(\theta)$mm and the relative permittivity of the object is $\varepsilon_r = 4.5$ is considered. The final reconstructed shapes by SADDE and DDE at the 300th generation are compared to the exact shape in Figure 4. Figure 5 shows that SADDE the relative errors of the shape function and permittivity decrease quickly and good convergences are achieved within 100 generation. The r.m.s. error of shape function for SADDE and DDE are about 1.05% and 2.96% in the final generation, respectively. The relative error for permittivity by SADDE and DDE are both less than 1%. It is clear that the SADDE outperforms DDE.

In the second example, let us consider the problem for dielectric cylinder with high permittivity. The shape function of this object is given by $F(\theta) = 29.75 + 5.95\cos(3\theta)$mm and the relative permittivity of the object is $\varepsilon_r = 8.0$. The reconstructed images at different generations and the relative error of the final example are shown in Figures 6 and 7, respectively. As shown in Figure 7, the r.m.s. error of shape function for SADDE and DDE are about 1.87% and 2.10% in the final generation, respectively. The relative error for permittivity by SADDE and DDE are both less than 1%. From the reconstructed results of this example, we conclude the proposed method is able to reconstruct buried dielectric cylinder successfully when the dielectric object with high-contrast permittivity.

To investigate the sensitivity of the imaging algorithm against random noise, the additive white Gaussian noise of zero mean with standard deviation σ_g is added into the scattered electric fields to mimic the measurement errors.

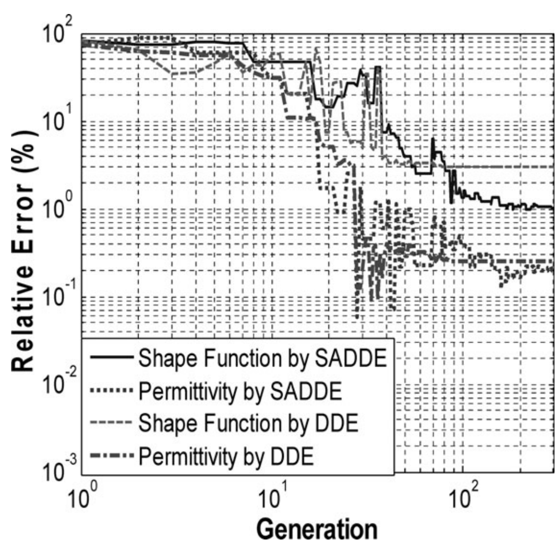

Figure 5 Error value versus generation for example 1 by DDE and SADDE, respectively.

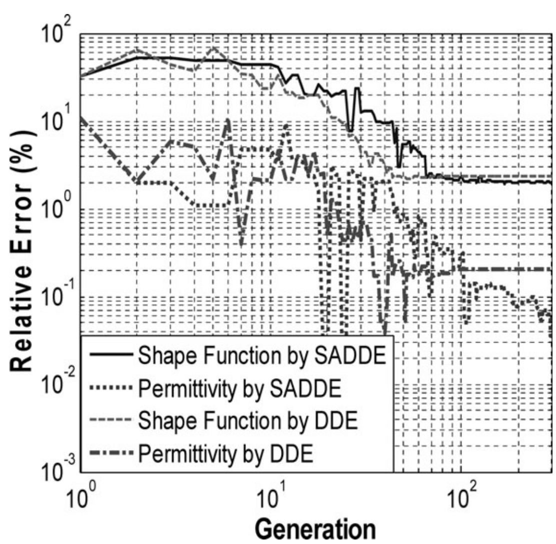

Figure 7 Error value versus generation for example 2 by DDE and SADDE, respectively.

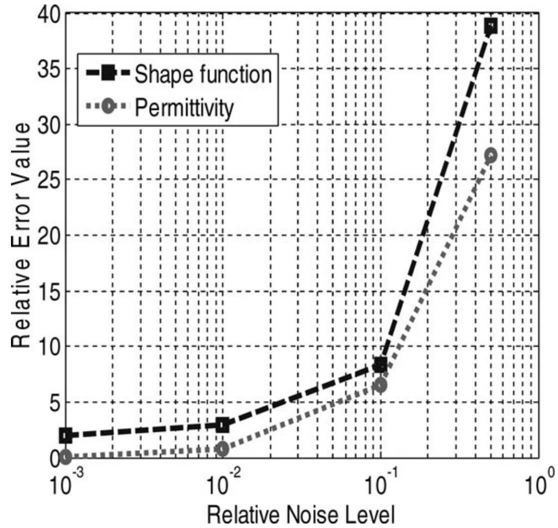

Figure 8 Shape error and relative permittivity errors as functions of RNL.

The relative noise level (RNL) is defined as:

$$\mathrm{RNL} = \frac{\sigma_g}{\sqrt{\dfrac{\sum_{n=1}^{Ni}\sum_{m=1}^{Mi}\sum_{q=0}^{Q}\left|E_z^{\exp}(n,m,q\,\Delta t)\right|^2}{(N_i)(M_i)(Q+1)}}} \tag{13}$$

The relative noise level of 10^{-3}, 10^{-2}, 10^{-1}, and 0.5 are used in SADDE for simulation purpose. Figure 8 shows the reconstructed results under the condition that the experimental scattered field is contaminated by the noise. It could be observed that good reconstruction has been obtained for shape of the dielectric cylinder when the relative noise level is below 10^{-1}.

From the reconstructed results this object, we conclude the SADDE scheme can be used to reconstruct dielectric cylinder. For complex shapes, it is found that SADDE has better reconstruction results than DDE does.

V. CONCLUSIONS

In this article, we study the time domain inverse scattering of an arbitrary cross section dielectric cylinder. Numerical results show that results by SADDE in accurate reconstruction even when noisy measurements are considered. Although DDE shows slightly better convergence rate at the initial iterations, finally, SADDE leads to more precise reconstruction results for the same population size and total number of iterations. It should be mentioned that this comparative study is indicative and its conclusion should not be considered generally applicable in all inverse scattering problems.

REFERENCES

1. F. Soldovieri, F. Ahmad, and R. Solimene, Validation of microwave tomographic inverse scattering approach via through-the-wall experiments in semicontrolled conditions, IEEE Trans Geosci Remote Sensing 8 (2011), 123–127.
2. A. Brancaccio and G. Leone, Multimonostatic shape reconstruction of two-dimensional dielectric cylinders by a Kirchhoff-based approach, IEEE Trans Geosci Remote Sensing 48 (2010), 3152–3161.
3. C.H. Sun, C.L. Liu, K.C. Chen, C.C. Chiu, C.L. Li, and C.C. Tasi, Electromagnetic transverse electric wave inverse scattering of a partially immersed conductor by steady-state genetic algorithm, Electromagnetics 28 (2008), 389–400.
4. L. Li, W. Zhang, and F. Li, Derivation and discussion of the SAR migration algorithm within inverse scattering problem: Theoretical analysis, IEEE Trans Geosci Remote Sensing 48 (2011), 415–422.
5. C.H. Sun and C.C. Chiu, Electromagnetic imaging of buried perfectly conducting cylinders targets using the dynamic differential evolution, Int J RF Microwave Comput-Aided Eng 22 (2012), 141–146.
6. X. Chen, Subspace-based optimization method for solving inverse-scattering problems, IEEE Trans Geosci Remote Sensing 48 (2010), 42–49.
7. C.C. Chiu and C.H. Sun, A study of microwave imaging for a metallic cylinder, Int J RF Microwave Comput-Aided Eng 22 (2012), 632–638.
8. C.H. Sun, C.C. Chiu, and C.J. Lin, Image reconstruction of inhomogeneous biaxial dielectric cylinders buried in a slab medium, Int J Appl Electromagnetics Mech 34 (2010), 33–48.
9. C.H. Sun, C.L. Li, C.C. Chiu, and C.J. Lin, Electromagnetic imaging for inhomogeneous dielectric cylinder buried in a slab medium, Tamkang J Sci Eng 12 (2009), 67–72.
10. M. Donelli and A. Massa, A computational approach based on a particle swarm optimizer for microwave imaging of two-dimensional dielectric scatterers, IEEE Trans Microwave Theory Tech 53 (2006), 1761–1776.
11. M. Donelli, G. Franceschini, A. Martini, and A. Massa, An integrated multiscaling strategy based on a particle swarm algorithm for inverse scattering problems, IEEE Trans Geosci Remote Sensing 44 (2006), 298–312.
12. X.-M. Zhong, C. Liao, and W. Chen, Image reconstruction of arbitrary cross section conducting cylinder using UWB pulse, J Electromagnetic Waves Appl 21 (2007), 25–34.
13. C.H. Sun, C.L. Li, C.C. Chiu, and C.H. Huang, Time domain image reconstruction for a buried 2D homogeneous dielectric cylinder using NU-SSGA, Res Nondestructive Eval 22 (2011), 1–15.
14. C.C. Chiu, C.H. Sun, and W.L. Chang, Comparison of particle swarm optimization and asynchronous particle swarm optimization for inverse scattering of a two-dimensional perfectly conducting cylinder, Int J Appl Electromagnetics Mech 35 (2011), 249–261.
15. C.H. Sun, C.C. Chiu, C.L. Li, and C.H. Huang, Time domain image reconstruction for homogenous dielectric objects by dynamic differential evolution, Electromagnetics 30 (2010), 309–323.
16. A. Semnani, M. Kamyab, and I.T. Rekanos, Reconstruction of one-dimensional dielectric scatterers using differential evolution and particle swarm optimization, IEEE Geosci Remote Sensing Lett 6 (2009), 671–675.
17. I.T. Rekanos, Shape reconstruction of a perfectly conducting scatterer using differential evolution and particle swarm optimization, IEEE Trans Geosci Remote Sensing 46 (2008), 1967–1974.
18. M. Pastorino, Stochastic optimization methods applied to microwave imaging: A review, IEEE Trans Antennas Propag 55 (2007), 538–548.
19. P. Rocca, M. Benedetti, M. Donelli, D. Franceschini, and A. Massa, Evolutionary optimization as applied to inverse scattering problems, Inverse Problems 925 (2009), 1–42.

20. C.H. Sun, C.C. Chiu, and C.L. Li, Time-domain inverse scattering of a two-dimensional metallic cylinder in slab medium using asynchronous particle swarm optimization, Prog Electromagn Res M. PIER M 14 (2010), 85–100.
21. C.C. Chiu, C.H. Sun, C.L. Li, and C.H. Huang, Comparative study of some population-based optimization algorithms on inverse scattering of a two-dimensional perfectly conducting cylinder in slab medium, IEEE Trans Geosci Remote Sensing.
22. J. Brest, S. Greiner, B. Boskovic, M. Mernik, and V. Zumer, Self-adapting control parameters in differential evolution: Comparative study on numerical benchmark problems, IEEE Trans Evol Comp 10 (2006), 646–657.
23. S.K. Goudos, K. Siakavara, T. Samaras, E.E. Vafiadis, and J.N. Sahalos, Self-adaptive differential evolution applied to real-valued antenna and microwave design problems, IEEE Trans Antennas Propag 59 (2011), 1286–1298.
24. M.W. Chevalier, R.J. Luebbers, and V.P. Cable, FDTD local grid with material traverse, IEEE Trans Antennas Propag 45 (1997), 3.
25. C. de Boor, A practical guide to splines, Springer-Verlag, New York, 1978.
26. K. Yee, Numerical solutions of initial boundary value problems involving Maxwell's equations in isotropic media, IEEE Trans Antennas Propagation AP-14 (1996), 302–307.
27. C.L. Li, C.W. Liu, and S.H. Chen, Optimization of a PML absorber's conductivity profile using FDTD, Microwave Opt Technol Lett 37 (2003), 380–383.
28. R. Storn and K. Price, Differential evolution—A simple and efficient adaptive scheme for global optimization over continuous spaces, Technical Report TR-95-012, International Computer Science Institute, Berkeley, 1995.
29. W. Chien and C.C. Chiu, Cubic-Spline expansion with GA for a partially immersed conducting cylinder, IEICE Trans Electron E88-C (2005), 2223–2228.
30. W. Chien and C.C. Chiu, Cubic-spline expansion with GA for half-space inverse problems, Appl Computat Electromagnetics Soc J 20 (2005), 136–143.

BIOGRAPHIES

Chi-Hsien Sun received MSEE and PhD degrees in electrical engineering from Tamkang University, Taipei, Taiwan, in 2008 and 2012, respectively. Since 2012, he has been a postdoctoral with the Department of Electronic and Computer Engineering, National Taiwan University of Science and Technology. His special interests include theoretical and computational electromagnetics, and application of various optimization schemes such as the steady state genetic algorithm (SSGA), particle swarm optimization (PSO), dynamic differential evolution (DDE), self-adaptive dynamic differential evolution (SADDE), and the Taguchi method in electromagnetics. E-mail: laisingsun@yahoo.com.tw

Chien-Ching Chiu received his BSCE degree from National Chiao Tung University, Hsinchu, Taiwan, in 1985 and his MSEE and PhD degrees from National Taiwan University, Taipei, in 1987 and 1991, respectively. From 1987 to 1989, he was a communication officer with the ROC Army Force. In 1992 he joined the faculty of the Department of Electrical Engineering, Tamkang University, where he is now a professor. From 1998 to 1999, he was a visiting scholar at the Massachusetts Institute of Technology, Cambridge, and the University of Illinois at Urbana-Champaign. He is a visiting professor with the University of Wollongong, Australia, in 2006. Moreover, he was a visiting professor with the University of London, United Kingdom, in 2011. His current research interests include microwave imaging, numerical techniques in electromagnetics, indoor wireless communications, and ultrawideband communication systems. He has published more than 100 journal papers on inverse scattering problems, communication systems and optimization algorithms.